Monthly Notices of the ROYAL ASTRONOMICAL SOCIETY

MNRAS **541,** 1774–1781 (2025) https://doi.org/10.1093/mnras/staf859
Advance Access publication 2025 May 27

The very high X-ray polarization of accreting black hole IGR J17091−3624 in the hard state

Melissa Ewing [1★] Maxime Parra [2] Guglielmo Mastroserio [3] Alexandra Veledina [4,5] Adam Ingram [1] Michal Dovčiak [6] Javier A. García [7,8] Thomas D. Russell [9] Maria C. Baglio [10] Juri Poutanen [4] Oluwashina Adegoke,[8] Stefano Bianchi [11] Fiamma Capitanio [12] Riley Connors,[13] Melania Del Santo [9] Barbara De Marco [14] María Díaz Trigo [15] Poshak Gandhi [16] Maitrayee Gupta [6] Chulsoo Kang [2] Elias Kammoun [8] Vladislav Loktev [4,17] Lorenzo Marra [12] Giorgio Matt [11] Edward Nathan [8] Pierre-Olivier Petrucci [18] Megumi Shidatsu [2] James F. Steiner [19] Francesco Tombesi [20,21,22] and Federico M. Vincentelli [16]

Affiliations are listed at the end of the paper

Accepted 2025 May 22. Received 2025 May 22; in original form 2025 March 31

ABSTRACT

We report the first detection of the X-ray polarization of the transient black hole X-ray binary IGR J17091−3624 taken with the *Imaging X-ray polarimetry Explorer* (*IXPE*) in 2025 March, and present the results of an X-ray spectropolarimetric analysis. The polarization was measured in the 2–8 keV band with 5.2 σ statistical confidence. We report a polarization degree (PD) of 9.1 ± 1.6 per cent and a polarization angle of $83^\circ \pm 5^\circ$ (errors are 1 σ confidence). There is a hint of a positive correlation of PD with energy that is not statistically significant. We report that the source is in the corona-dominated hard state, which is confirmed by a hard power-law-dominated spectrum with weak reflection features and the presence of a Type-C quasi-periodic oscillation at ~ 0.2 Hz. The orientation of the emitted radio jet is not known, and so we are unable to compare it with the direction of X-ray polarization, but we predict the two to be parallel if the geometry is similar to that in Cygnus X-1 and *Swift* J1727.8−1613, the two hard state black hole binaries previously observed by *IXPE*. In the Comptonization scenario, the high observed PD requires a very favourable geometry of the corona, a high inclination angle (supported by the presence of a dip in the light curve) and possibly a mildly relativistic outflow and/or scattering in an optically thick wind.

Key words: accretion, accretion discs – polarization – stars: black holes – X-rays: binaries.

1 INTRODUCTION

A black hole (BH) X-ray binary (XRB) is a system, whereby a stellar-mass BH accretes matter from a companion star, producing an extremely high X-ray flux. They are categorized into transient or persistent systems, where transient systems exhibit outbursts followed by quiescence and persistent systems maintain a steady flux above a quiescent level. In both cases, we observe spectral state transitions (Fender, Belloni & Gallo 2004; Done, Gierlinski & Kubota 2007; Belloni 2010). In transient systems, the outburst begins in the hard state, which is dominated by the Comptonization of photons from a quasi-thermal accretion disc (Novikov & Thorne 1973; Shakura & Sunyaev 1973) or internal synchrotron photons (Malzac & Belmont 2009; Poutanen & Vurm 2009; Veledina, Poutanen & Vurm 2011) in a hot cloud of electrons known as the 'corona' (Sunyaev & Titarchuk 1985). A steady compact jet is launched from the system during the hard state. The system then transitions through the intermediate state, where both the disc and corona are prominently observed in the spectrum, to the soft state, where now the spectrum is dominated by the disc and the compact jet is quenched. Again transitioning through intermediate states, the source moves back to the hard state and then quiescence. In the case of persistent sources, we observe these spectral transitions without the flux dropping to quiescence.

Because XRBs cannot be spatially resolved, the geometry and position with respect to the disc of the hard X-ray corona is still a matter of debate (Poutanen, Veledina & Zdziarski 2018). Several models have been proposed such as the 'sandwich' model, whereby the corona is thought to result from energy dissipation occurring above and below the disc (Haardt & Maraschi 1993; Svensson & Zdziarski 1994), the 'magnetic flare' model (Galeev, Rosner & Vaiana 1979; Beloborodov 1999) with the localized energy dissipation regions above the disc, the 'jet-base' model (Markoff, Nowak & Wilms 2005) in which the corona is vertically extended at the base of the jet, the 'lamppost' model (Matt 1993) where a compact corona lies above the BH on its spin axis, and the 'truncated disc' model (Eardley, Lightman & Shapiro 1975; Esin, McClintock & Narayan 1997; Poutanen, Krolik & Ryde 1997), whereby the disc evaporates beyond a truncation radius into a large scale-height hot

★ E-mail: m.ewing2@newcastle.ac.uk

flow. Each of these models can produce the same spectra, and so it is vital that we collect more information on these systems in order to break this degeneracy.

With the launch of the *Imaging X-ray Polarimetry Explorer* (*IXPE*; Weisskopf et al. 2022), we now have access to linear X-ray polarization information in the 2–8 keV energy range. We can measure the polarization degree (PD) – the extent to which the source X-ray photons have aligned electromagnetic fields – and the polarization angle (PA) – the angle at which the electromagnetic fields align. The PD increases with asymmetry of the emission region; i.e. with larger (more edge-on) inclination and smaller aspect ratio (Schnittman & Krolik 2010; Ursini et al. 2021; Poutanen, Veledina & Beloborodov 2023). For Comptonized radiation, the PA aligns perpendicular to the major axis of the scattering region (i.e. the corona). This happens because photons scatter preferentially in the plane perpendicular to their polarization vector, and they experience more scatterings along the major axis due to its higher scattering optical depth (Sunyaev & Titarchuk 1985; Ursini et al. 2021; Ingram et al. 2023).

The first BH XRB observed by *IXPE* during a hard state was Cygnus X-1 (hereafter Cyg X-1), the brightest persistent BH XRB observed in the sky. Linear polarization was detected with a $> 20\,\sigma$ statistical confidence, with PD $= 4.0 \pm 0.2$ per cent and PA $= -20.^{\circ}7 \pm 1.^{\circ}4$ (Krawczynski et al. 2022). The PA was found to align with the direction of the radio jet, suggesting that the corona is perpendicular to the jet and elongated in the disc plane. This favours horizontally extended models such as the truncated disc model over those vertically extended, such as the lamppost or jet-base model. With a relatively low inclination angle of $i = 27.^{\circ}5 \pm 0.^{\circ}8$ inferred from optical observations of the binary (Miller-Jones et al. 2021), a low PD of ≈ 1 per cent was expected (Krawczynski & Beheshtipour 2022). One explanation of this high observed PD is that the corona is more inclined than the binary system. This could be due to a misalignment between the BH and binary spin axes giving rise to a warped disc. Another potential explanation is an outflowing corona; Poutanen et al. (2023) showed that a mildly relativistic bulk coronal electron velocity of $v \sim 0.4\,c$ can boost the PD to the observed value for an aligned system (see also Dexter & Begelman 2024). If the former model is true, then this suggests that a significant subset of observed systems will exhibit a low PD. If the latter is true, then this implies that a high PD is common in XRB systems observed in the hard state.

The second BH XRB observed by *IXPE* in the hard state was *Swift* J1727.8−1613, a transient source that was discovered after going into a bright outburst in 2023 (Veledina et al. 2023). Again it was found that the PD was ≈ 4 per cent and that the PA was aligned with the orientation of the radio jet (Wood et al. 2024). This outburst was the first time that X-ray polarization had been tracked across a hard to soft state transition, where the PD was found to slowly decrease across the transition and the PA stayed constant (Ingram et al. 2024). The PD was later seen to reduce dramatically in the soft state (Svoboda et al. 2024), before recovering to the same level as before in the reverse soft to hard state transition (Podgorný et al. 2024).

IXPE observations of Type-1 active galactic nuclei (AGNs) may also help constrain the properties of the X-ray corona, since current understanding suggests that the hard X-rays produced by AGNs originate from a corona similar to that found in X-ray binaries. The PA measurements of NGC 4151 (Gianolli et al. 2023, 2024), IC 4329A (Ingram et al. 2023), and MCG-05-23-16 (Marinucci et al. 2022) have been found to align with the radio jet or ionization cone, suggesting again that the corona is extended in the disc plane. The observed PD values are also rather high (~ 3 per cent for IC 4329A and ~ 5 per cent for NGC 4151), given that Type-1 AGNs are thought to be viewed from a fairly low inclination according to the unification scheme.

IGR J17091−3624 is a transient BH XRB first discovered in 2003 by *INTEGRAL* (Kuulkers et al. 2003), and is of particular interest due to its extraordinary variability behaviour. While IGR J17091−3624 exhibits all the spectral states of a typical XRB (Capitanio et al. 2012), it also displays 10 different exotic variability states (Altamirano et al. 2011; Capitanio et al. 2012; Court et al. 2017; Wang et al. 2024). This makes it one of two systems known to exhibit this behaviour, the other source being GRS 1915+105, which has exhibited 14 different variability states (Belloni et al. 2000), 7 of which in common with IGR J17091−3624, including a heartbeat-like pattern (Wang et al. 2024). These variability states were first hypothesized from observations of GRS 1915+105 as radiation pressure instabilities deriving from its high-Eddington accretion rates, but because IGR J17091−3624 has demonstrated the same variability states at a flux estimated to be ∼20–30 times lower, this model is now being questioned. For example, the presence of substantial wind outflows from the accretion disc might significantly influence these instability patterns, potentially stabilizing or suppressing the observed heartbeat oscillations (Janiuk et al. 2015).

Here we report the results of the *IXPE* observation of IGR J17091−3624 in the hard state, taken in March 2025. We also discuss two shorter simultaneous observations by the *Nuclear Spectroscopic Telescope ARray* (*NuSTAR*). In Section 2, we detail the data reduction procedure. In Section 3, we present the polarimetric analysis as well as spectropolarimetric fits. In Section 4, we discuss our results and in Section 5 we summarize our conclusions.

2 OBSERVATION AND DATA REDUCTION

2.1 *IXPE* data

IGR J17091−3624 was observed by *IXPE* on 2025 March 7–10 for a total elapsed time of ~ 300 ks (obsID: 0450201). We measured a mean count rate of ~ 1 count s^{-1} with a useful exposure time of ~ 160 ks.

IXPE is a joint NASA/Italian Space Agency mission launched on 2021 December 9 from the Kennedy Space Center. It consists of three identical gas pixel detector units (DUs) that record the spatial, energy, timing, and polarimetric information from each event within a 2–8 keV energy band. Specifications and observatory details can be found in Weisskopf et al. (2022).

We downloaded the cleaned Level 2 event files for each DU (Costa et al. 2001) from the High Energy Astrophysics Science Archive Research Center (HEASARC[1]). We used `ds9` to define a circular source region centred on the source with a radius of 60″, and a background region of an annulus centred on the source with an inner radius of 150″ and an outer radius of 300″. Using the latest version of IXPEOBSSIM (v31.0.3; Baldini et al. 2022), we used the `xpselect` tool to create source and background fits files filtered for these regions. For our model-independent analysis, we used the `pcube` algorithm to calculate the Stokes parameters for the source and background regions, and subtract the background Stokes parameters from the source. For the spectropolarimetric analysis, we used the `PHA` algorithm to extract Stokes I, Q, and U as a function of energy channel for the source and background region of each detector unit, employing the most recent calibration data base files

[1] https://heasarc.gsfc.nasa.gov/docs/ixpe/archive/

associated with the latest version of IXPEOBSSIM, using an energy bin width of 0.016 keV. Throughout our analysis, we do not employ track weightings, and the PA is defined as East of North.

2.2 *NuSTAR* data

NuSTAR (Harrison et al. 2013) observed the source twice during the *IXPE* exposure (obsID 81 002 342 008 and 81002342010). The observations started on 2025 March 7 at 14:00 UTC and on March 8 at 23:30 UTC, respectively, and each had a 20 ks exposure time. We used the `nupipeline` and `nuproducts` routines distributed from the `NuSTARDAS v2.1.4` release with the calibration files `20250310` to produce the event files and the energy spectra for both Focal Plane Modules (FPMs). We chose an extraction region of 100 arcsec centred on the peak of the source photon counts. The same size region positioned as close as possible to the source was chosen for the background extraction. After preliminary analysis suggested that the spectra were broadly consistent between the two observations, we combined the FPMA and FPMB spectra from the two observations, as well as their backgrounds and response files, using `addascaspec` from the FTOOLS package. This step was taken solely to improve signal-to-noise in the visualizations. For a detailed analysis, it is best to treat the different observations and FPMs separately.

3 RESULTS

3.1 Model-independent analysis

We first measured the 2–8 keV polarization using the IXPEOBSSIM algorithm `pcube`. We found PD = 9.1 ± 1.6 per cent and PA = 83° ± 5° (1 σ uncertainties), and we plot the statistical confidence contours in Fig. 1(a) (colour filled contours).

To check if there is a dependence of polarization properties with energy, we used the same algorithm to calculate the PD and PA over a span of energy bins. The results can be seen in Fig. 1(b), with the PA showing no apparent energy dependence. The PD shows a possible increase with energy, which we test in the following subsection.

During the *IXPE* observation, IGR J17091−3624 experienced a dip in the X-ray flux reaching as low as ∼0.2 count s^{-1} overall DUs, starting ∼150 ks into the observation, and lasting for ∼50 ks. We plot the light curve of the total observation in Fig. 2, where the dip can clearly be observed. To test any effects that this may have on the observed polarization, we calculated the polarization properties excluding the events within the dip, again utilizing the `pcube` algorithm. We found PD = 8.4 ± 1.8 per cent and PA = 86° ± 6°, which is consistent with the results calculated for the entire observation. We therefore conclude that due to the low number of counts contributed from the dip to the total observation, it does not have a significant effect on the observed polarization.

3.2 Spectropolarimetric analysis

Using XSPEC v12.14.1 (Arnaud 1996), we simultaneously fitted Stokes I, Q, and U with several basic models representing different polarization properties. The polarization results and fit statistics for each model can be found in Table 1. We include a multiplicative `constant` component in each fit to account for cross-calibration between the DUs. We first fit the data with a model consisting of `diskbb` (Mitsuda et al. 1984) and `powerlaw` components, representing a multi-temperature black-body accretion disc and a power law with specific photon flux $\propto E^{-\Gamma}$. The interstellar absorption was accounted for using the model `tbabs` with the relative abundances from Wilms, Allen & McCray (2000).

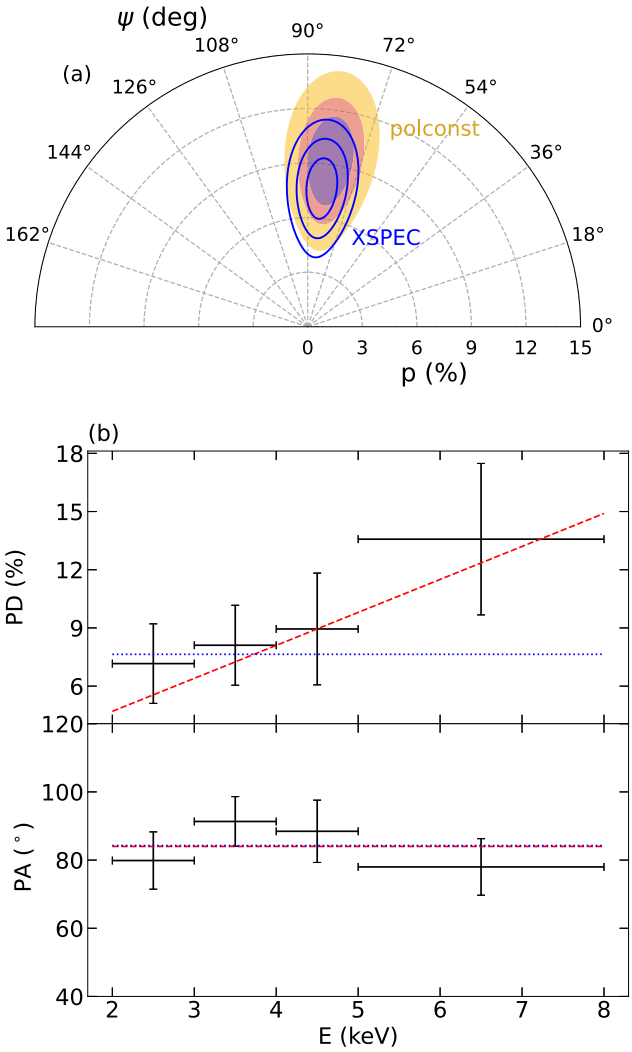

Figure 1. Polarimetric properties of IGR J17091−3624. (a) Constraints on the PD and PA (measured east of north) in the 2–8 keV band. The contours represent the confidence levels at 68, 90, and 99 per cent. The filled colour contours are the results of the unweighted, model-independent `pcube` algorithm. The blue contours are the results of an unweighted spectropolarimetric analysis within XSPEC. (b) Energy dependence of the observed PD (top) and PA (bottom) with 1 σ error bars as measured by the `pcube` algorithm. The red dashed lines represent the best-fitting energy dependent spectropolarimetric model (row 4 of Table 1), where the PD increases with energy while the PA remains constant. The blue dashed lines represent the best-fitting constant polarization model.

We first tested models with a constant, energy independent polarization using model `polconst` (rows 2–3 in Table 1). For the model including both disc and power-law components, i.e. `tbabs*polconst*(diskbb+powerlaw)`, we measure PD = 7.6 ± 1.8 per cent and PA = 84° ± 7° with a fit statistic χ^2/dof = 1320/1332. This inferred polarization is consistent with that measured using `pcube`, and we plot the resulting confidence contours in Fig. 1(a) (blue hollow contours).

We then fit the model without the `diskbb` component, i.e. `tbabs*polconst*(powerlaw)`, which returned a fit statistic of χ^2/dof = 1326/1334. We find that the polarization properties

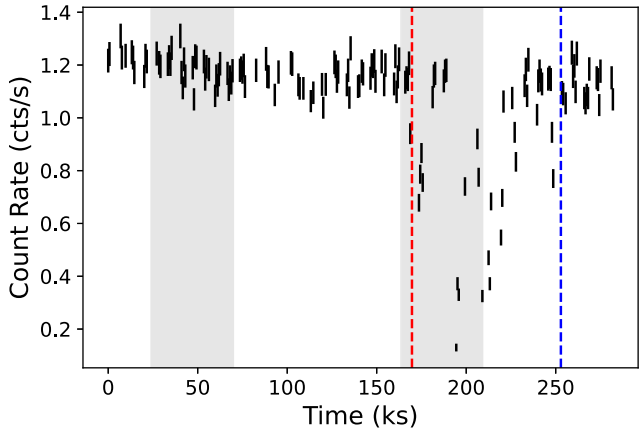

Figure 2. Light curve in counts per second of IGR J17091−3624 as observed by *IXPE* (black bars). The counts from each DU have been summed. The dip begins at the horizontal dashed red line, and ends at the horizontal blue dashed line. The shaded grey regions represent the two simultaneous *NuSTAR* observations. The error bars are derived from Poisson statistics.

between the two constant polarization models are consistent, and that the disc is only detected in the flux spectrum with a statistical confidence of 1.8 σ according to an F-test. We plot the unfolded Stokes I, Q, and U and the contributions to the fit statistic of the constant polarization model excluding the disc component in Fig. 3.

We then fit models to check for an energy dependence of the polarization properties by replacing `polconst` with `pollin`, which assumes a linear dependence of PD and PA with photon energy (rows 4–7 of Table 1). The linear relationship is described as $P(E) = P_1 + (E/\mathrm{keV} - 1) \times P_{\mathrm{slope}}$ where $P(E)$ is the energy dependent polarization property (i.e. either PD or PA), P_1 is the polarization property measured at 1 keV and P_{slope} is the gradient. We perform the fit under two different assumptions. The first assumption is that only the PD is variable with energy where the PA remains constant. This is achieved by freezing the slope parameter of PA to 0. In the second case, we assume that both PD and PA are energy dependent. We test these assumptions with (`tbabs*pollin*(diskbb+powerlaw)`) and without (`tbabs*pollin*(powerlaw)`) a disc component. We again find that the polarization results are consistent between models with and without the `diskbb` component, and so from here we continue our analysis considering the simpler models containing only the `powerlaw` component.

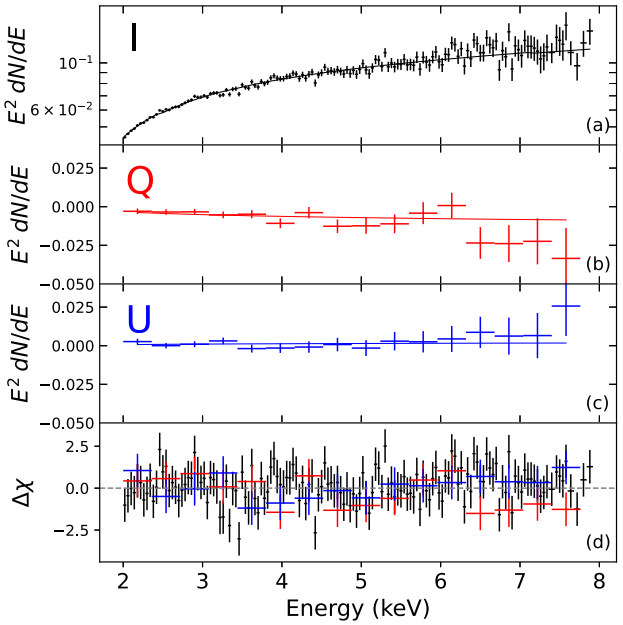

Figure 3. Spectral energy distribution of the constant polarization model (row 3 of Table 1). For plotting purposes only, we group the three DUs and employ energy rebinning to achieve a target signal to noise of 6 by binning no more than 9 channels (i.e. the `xspec` command `setplot rebin 6 9`). (a) Best-fitting spectral model for Stokes I (black line) with unfolded data (black crosses). (b) Best-fitting spectral model (red line) with unfolded Stokes Q (red crosses). (c) Best-fitting spectral model (blue line) with unfolded Stokes U (blue crosses). (d) Contributions to fit statistic χ. $\mathrm{d}N/\mathrm{d}E$ is in units of photons $\mathrm{cm}^{-2}\ \mathrm{s}^{-1}\ \mathrm{keV}^{-1}$.

To test if a polarization linearly dependent on energy is preferred to a constant polarization, we perform F-tests between the `polconst` model and the `pollin` model under the two aforementioned assumptions. The first test assuming only PD varies yields $F = 2.93$, meaning the variable PD is only preferred by 1.7 σ. Similarly for an F-test where PD and PA are free to vary, this model is only preferred to the constant polarization model by 1.3 σ. Although there is a hint of positive trending of PD with energy, no significant energy dependence of polarization properties has been detected.

We note that, although the `pcube` and `polconst` measurements of PD are consistent within 1 σ confidence, the `polconst` estimate is systematically lower (see e.g. Fig. 1a). This is likely because the

Table 1. Model fitting results showing PD, PA, hydrogen column density (N_{H}), power-law index (Γ), peak disc blackbody temperature (kT_{bb}), and chi-square per degree of freedom (χ^2/dof).

Model	PD (per cent)		PA (deg)		N_{H} (10^{22} cm^{-2})	Γ	kT_{bb} (keV)	χ^2/dof
`pcube`	9.1 ± 1.6		83 ± 5		–	–	–	–
`polconst*tbabs*(diskbb+po)`	7.6 ± 1.8		84 ± 7		$2.3^{+0.9}_{-0.8}$	$1.56^{+0.15}_{-0.28}$	$0.48^{+0.51}_{-0.11}$	1320/1332
`polconst*tbabs*po`	7.6 ± 1.8		84 ± 7		$1.39^{+0.15}_{-0.15}$	$1.58^{+0.04}_{-0.04}$	–	1326/1334
`pollin*tbabs*(diskbb+po)`	PD_1	3^{+5}_{-3}	PA_1	84 ± 7	$2.0^{+1.8}_{-0.7}$	$1.52^{+0.18}_{-0.17}$	$0.54^{+0.47}_{-0.16}$	1318/1331
	$\mathrm{PD}_{\mathrm{slope}}$	$1.6^{+1.5}_{-1.6}$	$\mathrm{PA}_{\mathrm{slope}}$	0.0				
`pollin*tbabs*po`	PD_1	3^{+5}_{-3}	PA_1	84 ± 7	$1.39^{+0.15}_{-0.15}$	$1.59^{+0.02}_{-0.04}$	–	1323/1333
	$\mathrm{PD}_{\mathrm{slope}}$	$1.7^{+1.5}_{-1.6}$	$\mathrm{PA}_{\mathrm{slope}}$	0.0				
`pollin*tbabs*(diskbb+po)`	PD_1	3^{+5}_{-3}	PA_1	90^{+10}_{-16}	$2.0^{+1.8}_{-0.7}$	$1.52^{+0.16}_{-0.17}$	$0.54^{+0.47}_{-0.16}$	1317/1330
	$\mathrm{PD}_{\mathrm{slope}}$	$1.8^{+1.4}_{-1.7}$	$\mathrm{PA}_{\mathrm{slope}}$	-2^{+4}_{-3}				
`pollin*tbabs*po`	PD_1	3^{+5}_{-3}	PA_1	90^{+17}_{-18}	$1.39^{+0.15}_{-0.15}$	$1.59^{+0.04}_{-0.04}$	–	1323/1332
	$\mathrm{PD}_{\mathrm{slope}}$	$1.8^{+1.4}_{-1.7}$	$\mathrm{PA}_{\mathrm{slope}}$	$-1.6^{+5.2}_{-1.6}$				

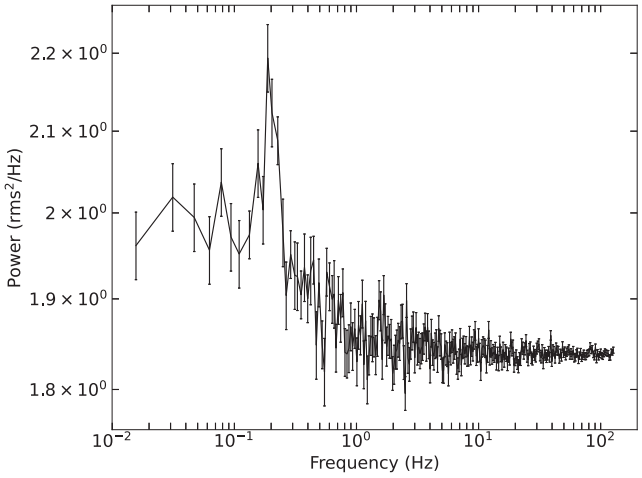

Figure 4. Power spectrum of the *IXPE* observation in the 2–8 keV band, calculated in fractional rms normalization, where Poisson noise has not been subtracted. The input light curve was binned in 1/256 s time bins and the power spectrum was averaged over a segment size of 64 s. Logarithmic rebinning was applied (with the geometric rebinning parameter set to $f = 0.2$).

PD is increasing with energy, as has been observed for other higher signal to noise data sets (e.g. Ingram et al. 2024), and is hinted at here but with low statistical confidence. The `polconst` model has, by design, constant PD and so the best-fitting PD value is weighted towards the lower energies, for which there are more counts. The `pcube` algorithm, in contrast, calculates the polarization properties averaged over the 2–8 keV bandpass (weighted by flux). To illustrate this, we plot in Fig. 1(b) the best-fitting PD and PA as a function of energy for our `polconst` (blue) and `pollin` (red) models. We see that, as expected, `pollin` agrees with the `pcube` points, whereas the `polconst` PD is slightly lower (whilst still within 2 σ uncertainties). We therefore adopt the `pcube` values as the best estimate of the 2–8 keV PD and PA.

3.3 State classification

For all models, we find that the hydrogen column density is in the range $N_{\rm H} \approx (1.4 - 2.3) \times 10^{22}$ cm^{-2} (consistent with previous measurements; Wang et al. 2024) and the power-law index is $\Gamma \approx 1.6$ (see Table 1). These values are consistent with that seen in Wang et al. (2024). This photon index indicates that IGR J17091−3624 was in the hard state during the *IXPE* observation. To further consolidate the hard-state classification, we also studied the timing properties. We created a light curve from all DUs with time bins of 1/256 s duration, and filtered the events such that they coincided with when all the DUs were in a good time interval (GTI). We then created a power spectrum averaged over a segment length of $T_{\rm seg} = 64$ s using the STINGRAY python package (Huppenkothen et al. 2019). It is clear from Fig. 4 that a Type-C quasi-periodic oscillation (QPO) is present at ~ 0.2 Hz. Based on this combination of spectral and timing evidence, we conclude that the source is in a hard state and that the X-ray flux is dominated by the corona.

We also considered the *NuSTAR* observations taken during the *IXPE* exposure (see the grey shaded regions in Fig. 2). We find that the energy spectrum in the 3–79 keV *NuSTAR* energy range is dominated by the Comptonized emission, such that a disc component is not required to fit the spectrum. Fig. 5 shows the results of fitting the combined spectrum of the two *NuSTAR* observations with the model `tbabs*nthComp`, where `nthcomp` is a thermal

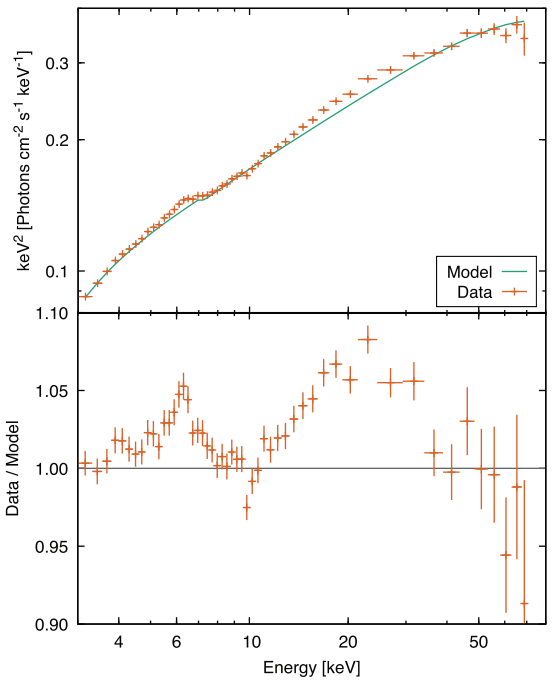

Figure 5. Unfolded *NuSTAR* energy spectrum fitted with the model `tbabs*nthComp` (top panel) and the corresponding residuals (bottom panel). FPMA and FPMB data are grouped for plotting purposes.

Comptonization model (Zdziarski, Johnson & Magdziarz 1996). We fix the hydrogen column density to $N_{\rm H} = 1.1 \times 10^{22}$ cm^{-2}, the seed blackbody photon temperature to $kT_{\rm bb} = 0.1$ keV, and the coronal electron temperature to $kT_{\rm e} = 40$ keV. This electron temperature is motivated by preliminary fits, but we note that a reliable constraint on $kT_{\rm e}$ requires a very detailed analysis beyond the scope of this paper. The measured photon index of $\Gamma = 1.607 \pm 0.002$ is consistent with what we measure with *IXPE* (see Table 1). The residuals to this fit clearly reveal an iron line and Compton hump indicative of reflection. The presence of a clear Compton hump contributes to our hard state classification, since the Compton hump is much weaker than the iron line for a soft illuminating spectrum (García et al. 2022).

Although we leave a rigorous fit with a reflection model to future work, the residuals being below 5 per cent from our preliminary fits (Fig. 5) suggests that reflection contributes ∼10–20 per cent of the flux in the *IXPE* band, with the rest dominated by the Comptonized emission. We leave a detailed spectropolarimetric analysis jointly considering the *IXPE* and *NuSTAR* observations and utilizing polarized reflection models for a follow-up paper.

4 DISCUSSION

We have presented an *IXPE* observation of IGR J17091−3624 in the hard state and find that the 2–8 keV polarization is PD = 9.1 ± 1.6 per cent and PA = 83° ± 5°. To-date no sufficiently high spatial resolution radio observations (i.e. with spatial resolutions ≪1 arcsec) have been performed on IGR J17091−3624, and no large-scale extended jet emission has been detected. As such, we are not able to compare the PA with the orientation of the jet in IGR J17091−3624. Additionally, simultaneous MeerKAT observations do not significantly detect radio polarization (Russell et al., in preparation), although, we note that a radio PA does not necessarily indicate the orientation of the jet (the magnetic field within the jet may be aligned in a variety of directions by different processes;

e.g. Curran et al. 2014, 2015). As such, we are unable to make any inference on the relative orientation of the corona, but for the purposes of this discussion, we will assume that it is extended in the disc plane as is indicated by the polarization aligning with the jet for all X-ray polarization detections of hard state BH XRBs and Seyfert-1 galaxies with resolved jets (Krawczynski et al. 2022; Gianolli et al. 2023; Ingram et al. 2023; Veledina et al. 2023).

Simultaneous Very Large Telescope (VLT) optical polarimetric observations show an increasing PD with frequency (2.9 ± 0.5 and 1.0 ± 0.3 per cent in the *R* and *I* bands, respectively; Baglio et al., in preparation), with a PA of $100^\circ \pm 5^\circ$ and $102^\circ \pm 8^\circ$, consistent with the *IXPE* PA within $2\,\sigma$. This behaviour aligns with recent findings on BH XRBs in their hard state, where the optical PA has been observed to be similar to the PA in the X-rays, for example, in Cyg X-1 (Krawczynski et al. 2022; Kravtsov et al. 2023), *Swift* J1727.8−0127 (Veledina et al. 2023) and GX 339−4 (Mastroserio et al. 2025), and the position angle of the radio jet in V404 Cyg (Kosenkov et al. 2017) and MAXI J1820+070 (Veledina et al. 2019). Similarly, also for IGR J17091−3624, we favour a scenario in which the optical radiation originates in the outer regions of the disc and is polarized through Thomson scattering in the disc atmosphere or wind.

The observed 2–8 keV PD of ≈9 per cent is significantly higher than what has been measured thus far for other sources in corona-dominated states (e.g. ∼4 per cent for both Cyg X-1 and Swift J1727−1613; Krawczynski et al. 2022; Veledina et al. 2023). Because the PD strongly depends on inclination, it is likely that IGR J17091−3624 is more highly inclined than the other sources. However, the inclination of IGR J17091−3624 is not well constrained. Reflection spectroscopy modelling yields estimates of fairly low inclination ($i \sim 30^\circ - 40^\circ$; Xu et al. 2017), whereas the presence of dipping in the light curve (e.g. our fig. 2 and Pahari et al. 2013) and wind signatures in the spectrum (Ponti et al. 2012; Parra et al. 2024; Wang et al. 2024), coupled with the absence of eclipses instead indicates that the inclination is in the range $60^\circ \lesssim i \lesssim 80^\circ$. The high amplitude of the Type-C QPO also points towards high inclination (Motta et al. 2015), consistent with the high inclination indicated by the high X-ray PD we observe here.

A PD of 9 per cent is high even for a high inclination source. To demonstrate this, we show in Fig. 6 the predicted PD as a function of inclination angle for a slab corona with seed photons provided from the side by a truncated disc (see fig. 1c of Poutanen et al. 2023). This geometry is consistent with our assumption that the corona is extended in the disc plane, and the parameters are chosen to maximise the predicted PD (see fig. 2 of Poutanen et al. 2023). We therefore note that these predictions should be seen as an upper limit of the expected PD from Comptonization, since any change to the assumed geometry (e.g. large coronal opening angles, significant inhomogeneities of the photosphere shape, etc.) would reduce the predicted PD – even if we were to drop our assumption of the PA aligning with the jet (Ursini et al. 2021). We use the radiative transfer code `compps` (Poutanen & Svensson 1996; see also Veledina & Poutanen 2022) and fix the photon index to $\Gamma = 1.6$ by adjusting the optical depth with inclination and electron temperature to maintain this value.

Additionally, we use a disc seed photon temperature of $kT_{\rm bb} = 0.1$ keV (typical for the hard-state sources and optimal to maximize the PD). The grey shaded area represents the 1 σ confidence interval of the observed PD. The black lines represent the case where the electrons in the corona have no bulk velocity ($\beta = v/c = 0$), only random thermal velocities. For the dashed line, we assume an electron temperature of $kT_{\rm e} = 40$ keV, which is consistent with the fairly low value of $kT_{\rm e}$ yielded by our initial fits to the *NuSTAR* data. We see that the observed PD is above this line for all viewing angles. However,

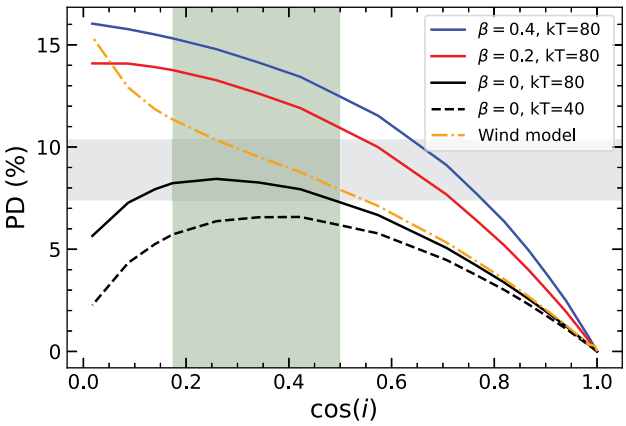

Figure 6. Predicted PD for a Comptonization model in a slab-corona as a function of the cosine of the inclination for different bulk velocities. The black, red and blue lines represent bulk velocities of $\beta = v/c = 0, 0.2$ and 0.4, respectively. The solid and dashed lines correspond to coronal temperatures of $kT_{\rm e} = 80$ and 40 keV, respectively. The coronal optical depth was adjusted to produce spectral slope $\Gamma = 1.6$. The orange dot–dashed line represents the PD influenced by scattering in a wind. The grey horizontal shaded area represents the limits on the observed PD measurement. The vertical green shaded region is the most likely range of inclination angles.

without a very detailed spectral analysis, $kT_{\rm e}$ is highly uncertain. We therefore also plot calculations assuming $kT_{\rm e} = 80$ keV as solid lines, which maximizes the predicted PD. We see that under this assumption, the $\beta = 0$ model is consistent with the measured PD within uncertainties as highlighted by the green shaded region.

A non-zero bulk outflow velocity, $\beta > 0$, of coronal electrons would increase the predicted PD due to relativistic aberration (Poutanen et al. 2023). We therefore plot examples of $\beta = 0.2$ and 0.4 in Fig. 6. We see that such values of the outflow velocity can reproduce the observed PD for much lower inclination angles. If the inclination of IGR J17091−3624 is $i \lesssim 60^\circ$ and the high PD results from bulk motion, this implies that other, higher inclination sources will be observed in future to have even higher PD.

Scattering in a disc wind adds another mechanism capable of affecting the polarization properties (Tomaru, Done & Odaka 2024; Nitindala, Veledina & Poutanen 2025), and IGR J17091−3624 is well known for strong wind signatures, albeit only in its exotic variability classes (Wang et al. 2024). The resulting PD depends on the optical depth of the wind, its characteristic opening angle, angular distribution and polarization of the incident X-ray emission. In Fig. 6, we show as the orange dot–dashed line an example for the PD boosted by scattering in the wind for the case of incident radiation corresponding to Comptonization in a slab corona of $kT_{\rm e} = 80$ keV producing a power-law spectrum with $\Gamma = 1.6$. We assumed a wind density profile following a Gaussian with opening angle $\alpha_{\rm w} = 20^\circ$ (Nitindala et al. 2025) and a mid-plane Thomson optical depth of $\tau_{\rm T} = 1$.

The assumed value of opening angle maximizes the predicted PD for $i \lesssim 80^\circ$, whereas the PD increases weakly with increasing optical depth (see figs 9c and 10c in Nitindala et al. 2025). Our assumed opening angle is also consistent with the existing observational evidence, since detections of highly ionized 'hot' absorption features in the X-ray spectrum have only been made for highly inclined sources, indicating that the wind is equatorial (Ponti et al. 2012; Parra et al. 2024). Such detections are typically only made in the soft state, because the highly ionized wind component becomes thermally unstable in the hard state, preventing the formation of lines.

In parallel, the last decade has seen a growing number of optical and infrared wind detections in the hard state, indicating that, at the very least, a 'cold' outflowing component remains active during the entire outburst in high-inclined sources (see e.g. Muñoz-Darias et al. 2016; Sanchez-Sierras & Munoz-Darias 2020; Panizo-Espinar et al. 2022, and references therein).

In IGR J17091-3624, the faintness of the optical counterpart is likely to prevent similar detections, but recent studies of this source in soft X-rays have shown the existence of an intermediate, 'warm' component that remains detectable even during canonical hard states (Gatuzz et al. 2020). While its column density ($N_H < 10^{22}\mathrm{cm}^{-2}$) alone is likely too low to significantly affect the PD, the majority of the column density lies in the 'hot' wind seen only in softer and exotic states (Wang et al. 2024). Leveraging the spectral resolution and sensitivity of newer instruments such as XRISM will allow future studies to precisely constrain the evolution of these components between the soft and the hard state, and with it, of the entire wind structure, allowing to draw more quantitative estimates of the impact of the wind on the PD.

The same process could affect the optical polarization as well. Our VLT polarimetric observations show an optical PD that increases slightly with frequency and a PA parallel to the X-ray PA measured with *IXPE*, suggesting that the polarization originates from scattering within the plane of the accretion disc. This scattering could occur either in the atmosphere of the viscously heated optically thick accretion disc itself or in a disc wind, and distinguishing between these two scenarios is not possible. A more detailed analysis will be presented in a forthcoming paper focused on the optical polarization properties of the source (Baglio et al., in preparation).

Reflection can also influence the observed PD, since the reflected emission can be more polarized than the directly observed coronal emission. The reflected emission is expected to be polarized perpendicular to the disc plane, thus aligning with the polarization of the direct coronal emission (which we are assuming to align with the jet). In this case, the overall 2–8 keV PD is given by

$$\mathrm{PD} = [(1 - R) \times \mathrm{PD_{cor}}] + R \times \mathrm{PD_{ref}}, \quad (1)$$

where R is the fraction of the 2–8 keV flux that is contributed by reflection, $\mathrm{PD_{cor}}$ is the PD of the corona and $\mathrm{PD_{ref}}$ is the PD of the reflection component. The maximum expected PD of the reflection component is ~ 20 per cent (Matt 1993; Poutanen, Nagendra & Svensson 1996; Podgorný et al. 2023), and our preliminary fits to the *NuSTAR* spectrum (Section 3.3) suggest $R \sim 0.1$–0.2, which is typical for the hard state (e.g. Krawczynski et al. 2022). Therefore, our observation of $\mathrm{PD} \approx 9$ per cent gives a lower limit for the PD of the directly observed emission of $\mathrm{PD_{cor}} \gtrsim 6$ per cent, which is still reasonably high compared with the expectations of thermal Compton scattering with no bulk velocity. More rigorous exploration of the physics of the corona will be provided by detailed spectropolarimetric fits that jointly consider the *IXPE* and *NuSTAR* data, which we leave to future work. Furthermore, future missions such as eXTP (Zhang et al. 2016) are capable of increasing the signal to noise of a similar observation. This would provide an enhanced view of the relationship between PD and energy, helping to distinguish between wind and bulk motion contributions.

5 CONCLUSIONS

We have obtained the first X-ray polarization measurement for the BH XRB IGR J17091−3624. The time- and energy-averaged $\mathrm{PD} = 9.1 \pm 1.6$ per cent and $\mathrm{PA} = 83^\circ \pm 5^\circ$ ($1\,\sigma$ errors) was measured with statistical confidence 5.2 σ using the model-independent `pcube` algorithm. We find no statistically significant dependence of the PD or PA on energy. From the shape of the energy spectrum, and the presence of a ∼0.2 Hz Type-C QPO in the power spectrum, we confirm that the source was observed in the hard state where the X-ray flux is dominated by the corona. Without the orientation of the radio jet we cannot confirm the orientation of the corona with respect to the disc, but we do find that the X-ray PA is consistent with the I and R band polarization within 2 σ confidence, as has previously been found for other BH XRBs (Krawczynski et al. 2022; Mastroserio et al. 2025). The very high observed PD requires IGR J17091−3624 to have a favourable coronal geometry and to be viewed from a favourable angle for it to be explained by standard thermal Comptonization models. If we are instead viewing from a lower inclination angle, the PD could have been boosted by the electrons in the corona having a mildly relativistic bulk outflow velocity, and/or by scattering in an optically thick disc wind. If this is true, we expect in future to observe other hard state BH XRBs with higher inclination angles that exhibit even higher PD.

ACKNOWLEDGEMENTS

ME and AI acknowledge support from the Royal Society. POP acknowledges financial support from the French Space National Agency (CNES) and the National Center of Scientifc Research (CNRS) via its 'Action Thématique' PEM. TDR and MCB are INAF IAF research fellows. GM and SB acknowledge financial support by the Italian Space Agency (Agenzia Spaziale Italiana, ASI) through the contract ASI-INAF-2022-19-HH.0. BDM acknowledges support via a Ramón y Cajal Fellowship (RYC2018-025950-I), the Spanish MINECO grants PID2023-148661NB-I00, PID2022-136828NB-C44, and the AGAUR/Generalitat de Catalunya grant SGR-386/2021. MD and MG thank GACR project 21–06825X for the support and institutional support from RVO:67985815. The work of GM and LM is partially supported by the PRIN 2022–2022LWPEXW – 'An X-ray view of compact objects in polarized light', CUP C53D23001180006. AV acknowledges support from the Academy of Finland grant 355672. Nordita is supported in part by NordForsk.This research has made use of data and/or software provided by the High Energy Astrophysics Science Archive Research Center (HEASARC), which is a service of the Astrophysics Science Division at NASA/GSFC and the High Energy Astrophysics Division of the Smithsonian Astrophysical Observatory.

DATA AVAILABILITY

IXPE data are publicly available from the HEASARC data archive (https://heasarc.gsfc.nasa.gov).

REFERENCES

Altamirano D. et al., 2011, ApJ, 742, L17
Arnaud K. A., 1996, in Jacoby G. H., Barnes J., eds, ASP Conf. Ser. Vol. 101, Astronomical Data Analysis Software and Systems V. Astron. Soc. Pac., San Francisco, p. 17
Baldini L. et al., 2022, SoftwareX, 19, 101194
Belloni T. M., 2010, in Belloni T., ed., Lecture Notes in Physics, Vol. 794, The Jet Paradigm – From Microquasars to Quasars. Springer Verlag, Berlin, p. 53
Belloni T., Klein-Wolt M., Méndez M., van der Klis M., van Paradijs J., 2000, A&A, 355, 271
Beloborodov A. M., 1999, ApJ, 510, L123
Capitanio F., Del Santo M., Bozzo E., Ferrigno C., De Cesare G., Paizis A., 2012, MNRAS, 422, 3130

Costa E., Soffitta P., Bellazzini R., Brez A., Lumb N., Spandre G., 2001, Nature, 411, 662
Court J. M. C., Altamirano D., Pereyra M., Boon C. M., Yamaoka K., Belloni T., Wijnands R., Pahari M., 2017, MNRAS, 468, 4748
Curran P. A. et al., 2014, MNRAS, 437, 3265
Curran P. A. et al., 2015, MNRAS, 451, 3975
Dexter J., Begelman M. C., 2024, MNRAS, 528, L157
Done C., Gierlinski M., Kubota A., 2007, A&A, 15, 1
Eardley D. M., Lightman A. P., Shapiro S. L., 1975, ApJ, 199, L153
Esin A. A., McClintock J. E., Narayan R., 1997, ApJ, 489, 865
Fender R. P., Belloni T. M., Gallo E., 2004, MNRAS, 355, 1105
Galeev A. A., Rosner R., Vaiana G. S., 1979, ApJ, 229, 318
García J. A., Dauser T., Ludlam R., Parker M., Fabian A., Harrison F. A., Wilms J., 2022, ApJ, 926, 13
Gatuzz E., Díaz Trigo M., Miller-Jones J. C. A., Migliari S., Castillo D., 2020, MNRAS, 491, 4857
Gianolli V. E. et al., 2023, MNRAS, 523, 4468
Gianolli V. E. et al., 2024, A&A, 691, A29
Haardt F., Maraschi L., 1993, ApJ, 413, 507
Harrison F. A. et al., 2013, ApJ, 770, 103
Huppenkothen D. et al., 2019, ApJ, 881, 39
Ingram A. et al., 2023, MNRAS, 525, 5437
Ingram A. et al., 2024, ApJ, 968, 76
Janiuk A., Grzedzielski M., Capitanio F., Bianchi S., 2015, A&A, 574, A92
Kosenkov I. A., Berdyugin A. V., Piirola V., Tsygankov S. S., Pallé E., Miles-Páez P. A., Poutanen J., 2017, MNRAS, 468, 4362
Kravtsov V. et al., 2023, A&A, 678, A58
Krawczynski H., Beheshtipour B., 2022, ApJ, 934, 4
Krawczynski H. et al., 2022, Science, 378, 650
Kuulkers E., Lutovinov A., Parmar A., Capitanio F., Mowlavi N., Hermsen W., 2003, Astron. Telegram, 149, 1
Malzac J., Belmont R., 2009, MNRAS, 392, 570
Marinucci A. et al., 2022, MNRAS, 516, 5907
Markoff S., Nowak M. A., Wilms J., 2005, ApJ, 635, 1203
Mastroserio G. et al., 2025, ApJ, 978, L19
Matt G., 1993, MNRAS, 260, 663
Miller-Jones J. C. A. et al., 2021, Science, 371, 1046
Mitsuda K. et al., 1984, PASJ, 36, 741
Motta S. E., Casella P., Henze M., Muñoz-Darias T., Sanna A., Fender R., Belloni T., 2015, MNRAS, 447, 2059
Muñoz-Darias T. et al., 2016, Nature, 534, 75
Nitindala A. P., Veledina A., Poutanen J., 2025, A&A, 694, A230
Novikov I. D., Thorne K. S., 1973, in Witt B., Witt C., eds, Black Holes (Les Astres Occlus). Gordon and Breach, New York, p. 343
Pahari M., Yadav J. S., Rodriguez J., Misra R., Bhattacharyya S., Pandey S. K., 2013, ApJ, 778, 46
Panizo-Espinar G. et al., 2022, A&A, 664, A100
Parra M., Petrucci P. O., Bianchi S., Gianolli V. E., Ursini F., Ponti G., 2024, A&A, 681, A49
Podgorný J., Dovčiak M., Goosmann R., Marin F., Matt G., Różańska A., Karas V., 2023, MNRAS, 524, 3853
Podgorný J. et al., 2024, A&A, 686, L12
Ponti G., Fender R. P., Begelman M. C., Dunn R. J. H., Neilsen J., Coriat M., 2012, MNRAS, 422, L11
Poutanen J., Svensson R., 1996, ApJ, 470, 249
Poutanen J., Vurm I., 2009, ApJ, 690, L97
Poutanen J., Nagendra K. N., Svensson R., 1996, MNRAS, 283, 892
Poutanen J., Krolik J. H., Ryde F., 1997, MNRAS, 292, L21
Poutanen J., Veledina A., Zdziarski A. A., 2018, A&A, 614, A79
Poutanen J., Veledina A., Beloborodov A. M., 2023, ApJ, 949, L10
Sanchez-Sierras J., Munoz-Darias T., 2020, A&A, 640, L3
Schnittman J. D., Krolik J. H., 2010, ApJ, 712, 908
Shakura N. I., Sunyaev R. A., 1973, A&A, 24, 337
Sunyaev R. A., Titarchuk L. G., 1985, A&A, 143, 374
Svensson R., Zdziarski A. A., 1994, ApJ, 436, 599
Svoboda J. et al., 2024, ApJ, 966, L35
Tomaru R., Done C., Odaka H., 2024, MNRAS, 527, 7047
Ursini F., Matt G., Bianchi S., Marinucci A., Dovčiak M., Zhang W., 2021, MNRAS, 510, 3674
Veledina A., Poutanen J., 2022, Polarization of Comptonized Emission in Slab Geometry, Zenodo. Available at: https://doi.org/10.5281/zenodo.7116125
Veledina A., Poutanen J., Vurm I., 2011, ApJ, 737, L17
Veledina A. et al., 2019, A&A, 623, A75
Veledina A. et al., 2023, ApJ, 958, L16
Wang J. et al., 2024, ApJ, 963, 14
Weisskopf M. C. et al., 2022, JATIS, 8, 026002
Wilms J., Allen A., McCray R., 2000, ApJ, 542, 914
Wood C. M. et al., 2024, ApJ, 971, L9
Xu Y. et al., 2017, ApJ, 851, 103
Zdziarski A. A., Johnson W. N., Magdziarz P., 1996, MNRAS, 283, 193
Zhang S. N. et al., 2016, in den Herder J.-W. A., Takahashi T., Bautz M., eds, Proc. SPIE Vol. 9905, Space Telescopes and Instrumentation 2016: Ultraviolet to Gamma Ray. SPIE, Bellingham, p. 99051Q

[1]*School of Mathematics, Statistics, and Physics, Newcastle University, Newcastle upon Tyne, NE1 7RU, UK*
[2]*Department of Physics, Ehime University, 2-5, Bunkyocho, Matsuyama, Ehime 790-8577, Japan*
[3]*Dipartimento di Fisica, Università degli Studi di Milano, Via Celoria 16, I-20133 Milano, Italy*
[4]*Department of Physics and Astronomy, University of Turku, FIN-20014 Turku, Finland*
[5]*Department of Astrophysics and Astroparticle Physics, Nordita, KTH Royal Institute of Technology and Stockholm University, Hannes Alfvéns väg 12, SE-10691 Stockholm, Sweden*
[6]*Astronomical Institute of the Czech Academy of Sciences, Boční II 1401, 14100 Praha, Czech Republic*
[7]*X-ray Astrophysics Laboratory, NASA Goddard Space Flight Center, Greenbelt, MD 20771, USA*
[8]*Cahill Center for Astrophysics, California Institute of Technology, 1216 East California Boulevard, Pasadena, CA 91125, USA*
[9]*Astrophysics and Astroparticles, INAF, Istituto di Astrofisica Spaziale e Fisica Cosmica, Via U. La Malfa 153, I-90146 Palermo, Italy*
[10]*INAF, Osservatorio Astronomico di Brera, Via Bianchi 46, I-23807 Merate (LC), Italy*
[11]*Dipartimento di Matematica e Fisica, Università degli Studi Roma Tre, Via della Vasca Navale 84, I-00146 Roma, Italy*
[12]*High Energy Astrophysics, INAF, Istituto di Astrofisica e Planetologia Spaziali, via del fosso del Cavaliere 100, I-00133 Roma, Italy*
[13]*Department of Physics, Villanova University, 800 E. Lancaster Avenue, Villanova, PA 19085, USA*
[14]*Departament de Fisíca, EEBE, Universitat Politècnica de Catalunya, Av. Eduard Maristany 16, E-08019 Barcelona, Spain*
[15]*ESO, Karl-Schwarzschild-Strasse 2, Garching bei München, D-85748, Germany*
[16]*School of Physics & Astronomy, University of Southampton, Southampton SO17 1BJ, UK*
[17]*Department of Physics, University of Helsinki, P.O. Box 64, FIN-00014 Helsinki, Finland*
[18]*Université Grenoble Alpes, CNRS, IPAG, F-38000 Grenoble, France*
[19]*Center for Astrophysics | Harvard & Smithsonian, 60 Garden St, Cambridge, MA 02138, USA*
[20]*Dipartimento di Fisica, Università degli Studi di Roma 'Tor Vergata', Via della Ricerca Scientifica 1, I-00133 Rome, Italy*
[21]*INAF, Osservatorio Astronomico di Roma, Via Frascati 33, I-00040 Monte Porzio Catone, Italy*
[22]*INFN, Sezione di Roma 'Tor Vergata', Via della Ricerca Scientifica 1, I-00133 Rome, Italy*

This paper has been typeset from a TEX/LATEX file prepared by the author.